research papers

Determination of the three-dimensional structure of dislocations in silicon by synchrotron white X-ray topography combined with a topo-tomographic technique

Seiji Kawado,[a]* Toshinori Taishi,[b] Satoshi Iida,[c] Yoshifumi Suzuki,[d] Yoshinori Chikaura[d] and Kentarou Kajiwara[e]

[a]X-ray Research Laboratory, Rigaku Corporation, Japan, [b]Faculty of Education, Shinshu University, Japan, [c]Faculty of Science, Toyama University, Japan, [d]Graduate School of Engineering, Kyushu Institute of Technology, Japan, and [e]Japan Synchrotron Radiation Research Institute, SPring-8, Japan. E-mail: kawado@rigaku.co.jp

The determination of the three-dimensional dislocation structure, *i.e.* the configuration and nature of the dislocations, in silicon by synchrotron white X-ray topography combined with a topo-tomographic technique is demonstrated. A [001]-oriented CZ-Si crystal of diameter $\sim$7 mm was fixed on a subsidiary goniometer with three rotation axes (ω, Rx, Ry) and x-y-z stages, keeping its growth axis parallel to the ω-axis. This goniometer was mounted on the swivel stage of the main diffractometer installed at the experimental hutch of beamline BL28B2 of SPring-8. After adjusting the (110) plane to be perpendicular to the incident white X-ray beam by observing transmission Laue patterns, the crystal was inclined by 4.3° so that the 004 Laue spot could be formed by 60 keV X-rays. Laue topographs observed by rotating the ω-axis of the subsidiary goniometer were recorded using X-ray films and a cooled CCD camera. The direction of the dislocation lines, Burgers vectors and glide planes were determined by following the variation in features of the dislocation images in the 004 Laue spot and by examining the contrast of the dislocation images in the Laue spots concerning the {111} and {022} planes. It is concluded that white X-ray topography combined with the ω-rotation technique is useful for clarifying the three-dimensional dislocation structure.

Keywords: synchrotron white X-ray topography; silicon; three-dimensional structure of dislocations.

1. Introduction

X-ray diffraction topography has been used to observe lattice defects in semiconductor single crystals such as Si, GaAs, InP *etc.* since the 1960s (Tanner, 1976; Bowen & Tanner, 1998; Authier, 2001). Techniques often used in laboratory experiments are transmission topography and double-crystal topography. Transmission topography is usually carried out with a topographic X-ray camera using the Lang method under easy operation (Lang, 1970). The camera has gradually become larger with increasing wafer size, and nowadays a topographic camera that accepts 300 mm Si wafers is widely used for observing process-induced defects such as slip dislocations and oxygen precipitates generated during thermal processes of the LSI device fabrication (Kawado, 2003).

The application of synchrotron radiation to X-ray diffraction topography has been developed in white X-ray topography and monochromatic X-ray topography (Lang, 1999). White X-ray topography has the advantage of acquiring defect images in several Laue spots at the same time even though high strain-sensitivity is not available. When higher sensitivity to strain is needed we can employ another method, synchrotron plane-wave X-ray topography, which reveals microdefects and minute strain due to impurity inhomogeneity in as-grown Si crystals (Ishikawa, 1989; Kudo *et al.*, 1997).

A three-dimensional characterization is often required in X-ray topography studies. At the early stage of the development of X-ray topography technology, stereo-topographs were often recorded as a pair in the hkl and $\bar{h}k\bar{l}$ reflections (Lang, 1959) or taken as a pair rotated by $\pm 8°$ about the diffraction vector (Haruta, 1965). Another technique is an application of section topography that enables us to determine the depth distribution of lattice defects, and this has been realized as step-scanned section topography (Andersen & Gerward, 1974; Kawado & Aoyama, 1979).

Recently, a new technique, 'topo-tomography', has been developed at beamline ID-19 of the ESRF, which combines tomographic and topographic imaging (Ludwig *et al.*, 2001). It has allowed us to analyze the configuration of individual dislocations inside a low-absorbing single crystal of high quality, *e.g.* a synthetic diamond. This technique is very sophisticated but is insufficient for determining the nature of individual dislocations such as their Burgers vectors and glide planes owing to a lack of information about their image contrast.

In the present paper we demonstrate how to determine the configuration and nature of dislocations in silicon by white X-ray topography combined with a topo-tomographic technique at beamline BL28B2 of the synchrotron radiation facility SPring-8 in Japan. The advantage of the present method is the ability to acquire information about the configuration of dislocations from the variation in their features observed in a specific Laue spot by the tomographic technique, in addition to information about the image contrast of the dislocations observed in several Laue spots by conventional white X-ray topography.

2. Experimental

As a test sample, a Si crystal, grown by the conventional Czochralski (CZ) method intentionally without enlarging its diameter in order to observe the features of dislocation generation and propagation easily, was employed. The seed used was a dislocation-free undoped [001]-oriented Si single crystal having dimensions of about 7 mm × 7 mm × 30 mm, and the portion of the sample grown along the [001] orientation, having a diameter of about 7 mm and a length of about 180 mm, was also undoped.

Fig. 1 shows the experimental set-up. A subsidiary goniometer, comprised of a sample holder, x-y stages, two swivel stages (Rx, Ry), a z-stage and a rotational stage (ω), was constructed for this experiment. The sample crystal fixed the seed down, keeping its growth axis [001] parallel to the ω-axis, on the sample holder of the subsidiary goniometer which was mounted on the swivel stage of the main diffractometer installed at the white X-ray topography station of beamline BL28B2 (Chikaura *et al.*, 2001; Imai *et al.*, 2003).

The portion of the sample to be observed was selected using the z-stage, and was then adjusted using the x-y stages so as not to be shifted by the ω-rotation. The sample was irradiated with a white X-ray beam of about 7 mm (H) × 4 mm (V), and transmission Laue patterns were observed on an ordinary fluorescent screen, which was fixed at the position of the film cassette on the counter arm of the main diffractometer, through a monitor camera. The (110) plane of the sample was adjusted so as to be perpendicular to the incident X-ray beam and with the [$1\bar{1}0$] orientation

horizontal. This angular position was designated as $\omega = 0$. In the cases of $\omega = 45, 90, 135$ and $180°$, the plane perpendicular to the incident X-ray beam corresponded to (100), $(1\bar{1}0)$, $(0\bar{1}0)$ and $(\bar{1}\bar{1}0)$, respectively.

Next, we inclined the sample, using the Rx stage of the main diffractometer, by $4.36°$ (Bragg angle) so that the 004 Laue spot could be formed by 60 keV X-rays. The ordinary fluorescent screen was replaced by a windowed fluorescent screen having a backing of lead, together with a cooled CCD camera. The position of the counter arm was arranged so that the 004 Laue spot could pass through the window of the fluorescent screen and could reach the CCD camera. This camera was comprised of a small fluorescent screen, a mirror, two convex lenses and a cooled CCD (10 mm × 10 mm, 1024 × 1024 pixels). Finally, we precisely adjusted the growth axis [001] of the sample crystal so as to be parallel to the ω-axis using the Rx and Ry stages of the subsidiary goniometer.

After the adjustment mentioned above, we observed enlarged images of the 004 Laue spot from the grown crystal, the seed and their interface region. Selecting the position to be observed, we examined the change in the image by rotating the ω-axis of the subsidiary goniometer in the range 0–180° at intervals of 2.4°, and recorded the image data on the hard disk of a personal computer connected to the CCD camera. Furthermore, we recorded several sets of Laue patterns on X-ray films (Agfa D2) by rotating the ω-axis at intervals of 45°. The distance between the sample and the film was 220 mm.

Analysis of the three-dimensional dislocation structure, *i.e.* the configuration and nature of dislocations observed in the sample, was performed as follows. The first step was to follow the variation in features of individual dislocations owing to the ω-rotation by reproducing their CCD images, in order to clarify the configuration of each dislocation and identify its image in the 004 spot taken at $\omega = 0$, 45, 90, 135 and 180°. The second step was to determine their Burgers vectors from the change in contrast of their images in several Laue spots recorded on the X-ray film at each ω-angle. The final step was to fix glide planes both from the configuration of the dislocations clarified by the first step and from the Burgers vectors determined by the second step.
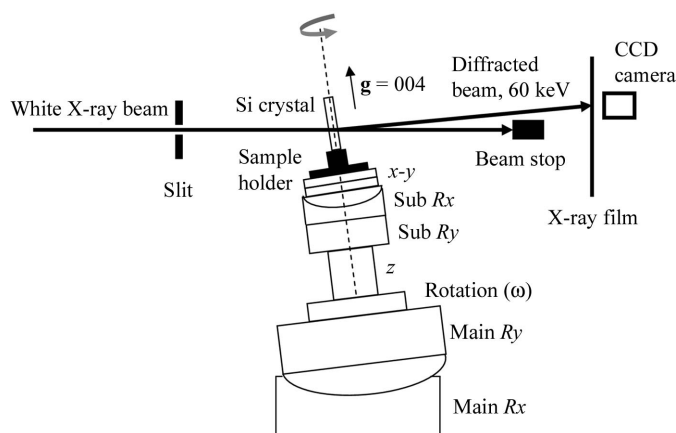

Figure 1
Schematic illustration of the experimental arrangement for synchrotron white X-ray topography combined with a topo-tomographic technique. The subsidiary goniometer is comprised of a sample holder and x-y, Rx, Ry, z and ω-rotation stages. Only the Rx and Ry swivel stages of the main diffractometer are drawn.

3. Results and discussion

Fig. 2 shows CCD images of the 004 spot obtained at $\omega = 0°$ from the grown crystal, the interface region and the seed. The grown crystal and seed regions were about 7.5 mm and 8 mm, respectively, from the interface. These images indicated the features of dislocation generation and propagation in the three portions of the sample. Many dislocations generated by thermal shock at the early stage of crystal growth were clearly observed in the close vicinity of the interface, together with frozen-in strain. The dislocation density was decreased by increasing the distance from the interface both in the grown crystal and seed regions. Detailed observation of dislocations in the portion of the seed at 6–10 mm away from the interface (the lower photograph in Fig. 2) is demonstrated in the following.

Figs. 3(a) and 3(b) show Laue patterns obtained from this specified portion of the seed in the cases of $\omega = 0°$ and $\omega = 45°$, respectively. Since the ω-rotation axis was parallel to the 004 **g**-vector, the 004 spot was always fixed at a constant position, while other Laue spots were moved by the ω-rotation. The spots concerning the {113} and {111} planes were observed at $\omega = 0$, 90 and 180°, and the spots concerning the {022} planes were observed at $\omega = 45$ and 135°. Since each spot recorded on the X-ray film possessed fine structure, they were enlarged using an optical microscope.

Fig. 4 shows a series of enlarged images in the 004 spot obtained at $\omega = 0$, 45, 90, 135 and 180°. Individual dislocations were clearly observed, and these configurations were naturally changed by the
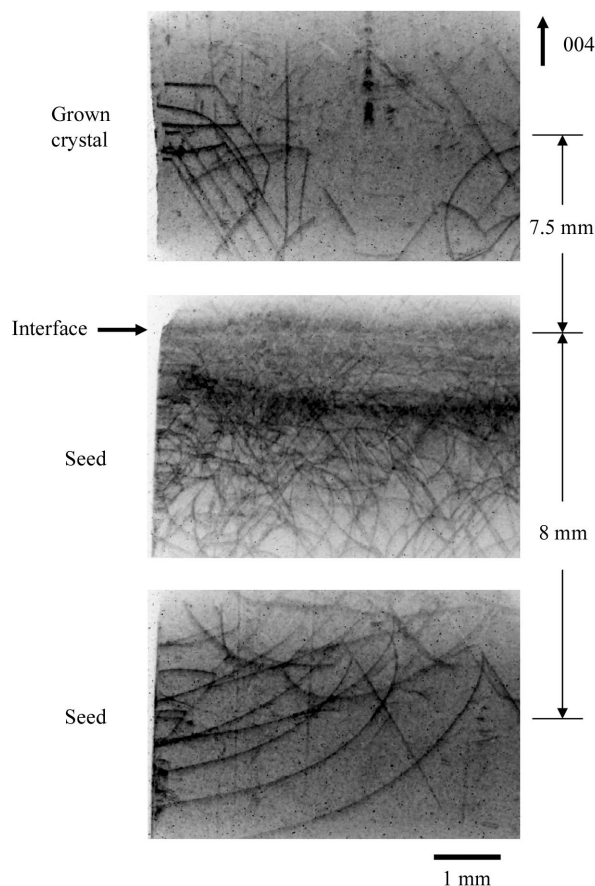

Figure 2
CCD images of the 004 spot obtained at $\omega = 0°$ from the grown-crystal region (upper), the interface region between the grown crystal and the seed (middle), and the seed region (lower). Very fine dark dots are attributable to video noise.

ω-rotation. Using the video images recorded with the CCD camera at ω-intervals of 2.4°, we carefully traced the images of the individual dislocations at each ω-angle. Here we identified five representative examples, and designated these dislocations as A, B, C, D and E.

It is well known that the slip system of the diamond lattice is $\mathbf{a}/2\langle 110\rangle/\{111\}$, where $\mathbf{a}$ is a translation vector, $\mathbf{a}/2\langle 110\rangle$ is a Burgers vector (designated as $\mathbf{b}$ hereafter) of a perfect dislocation, and $\{111\}$ is a slip plane (Hirth & Lothe, 1968). Therefore, we can determine the Burgers vector by examining the contrast of the dislocation images in four Laue spots concerning $\{111\}$ planes. However, the dislocation images occasionally overlapped with other images, and hence we added the $0\bar{2}2$ and 022 spots to the $1\bar{1}1$, $\bar{1}11$, $\bar{1}\bar{1}1$ and 111 spots. Fig. 5 shows enlarged images of these Laue spots which reveal the visibility of dislocations A to E. An example of possible overlapping images is the image of dislocation E in the 111 spot at $\omega = 90°$. Based on the criterion of no contrast at $\mathbf{g}\cdot\mathbf{b} = 0$ (Authier, 2001), where $\mathbf{g}$ is a diffraction vector, the Burgers vector was determined and the results are summarized in Table 1. Dislocations A, B and C have a Burgers vector of $\mathbf{a}/2[\bar{1}01]$, dislocation D has a Burgers vector of $\mathbf{a}/2[101]$ and dislocation E has a Burgers vector of $\mathbf{a}/2[0\bar{1}1]$.

Glide planes can be fixed on the basis of both the configuration of dislocation lines, determined from the dependence of dislocation images on the ω-rotation, and Burgers vectors, determined from the criterion for the image contrast. Curved dislocations A, B and C lie on (111) because they give straight-line images along $[\bar{1}\bar{1}2]$ at $\omega = 90°$. Since the Burgers vector $\mathbf{a}/2[\bar{1}01]$ of these dislocations also lies on (111), the glide plane is found to be (111), and consequently the nature of these dislocations is determined to be a mixed type. Both dislocations D and E give straight-line images along $[1\bar{1}2]$ at $\omega = 0°$. However, dislocation D gives curved images at $\omega = 45, 90, 135$ and $180°$, while dislocation E keeps straight-line images at these ω-angles. Curved dislocation D lies on $(\bar{1}11)$ and has a Burgers vector of $\mathbf{a}/2[101]$, and hence the glide plane is $(\bar{1}11)$ and the nature of this dislocation is a mixed type. On the other hand, straight dislocation E is found to be along $[1\bar{1}2]$ from the change in its direction by the ω-rotation. Since its Burgers vector is $\mathbf{a}/2[0\bar{1}1]$, the glide plane is $(\bar{1}11)$, and consequently the nature of this dislocation is determined to be a 30° type. The results of identification of the observed dislocations A to E are summarized in Table 1, and shown schematically in Fig. 6.

4. Conclusion

The combination of synchrotron white X-ray topography and a topo-tomographic technique provides a useful tool for determining the three-dimensional structure of individual dislocations in a [001]-oriented Si crystal, i.e. the direction of the dislocation line, its Burgers vector and the glide plane. To clarify the configuration of the dislocations, we need to fix the growth axis of the crystal
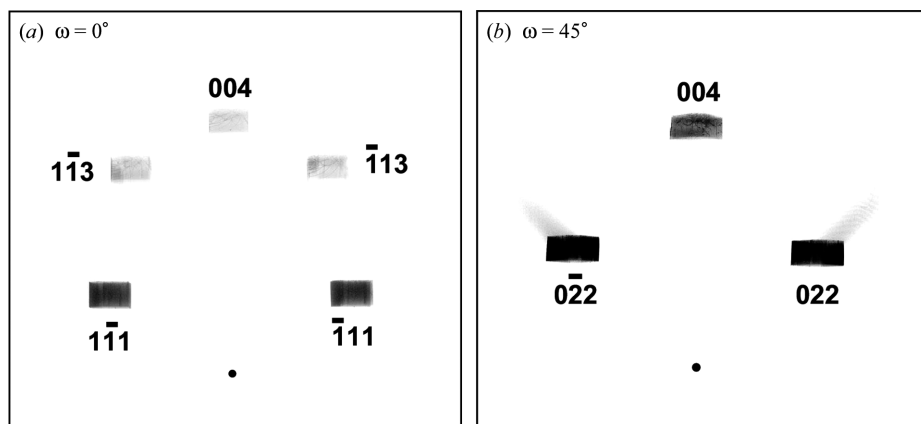

Figure 3
Laue patterns from the portion of the seed which is shown in the lower photograph in Fig. 2 at (a) $\omega = 0°$ and (b) $\omega = 45°$.
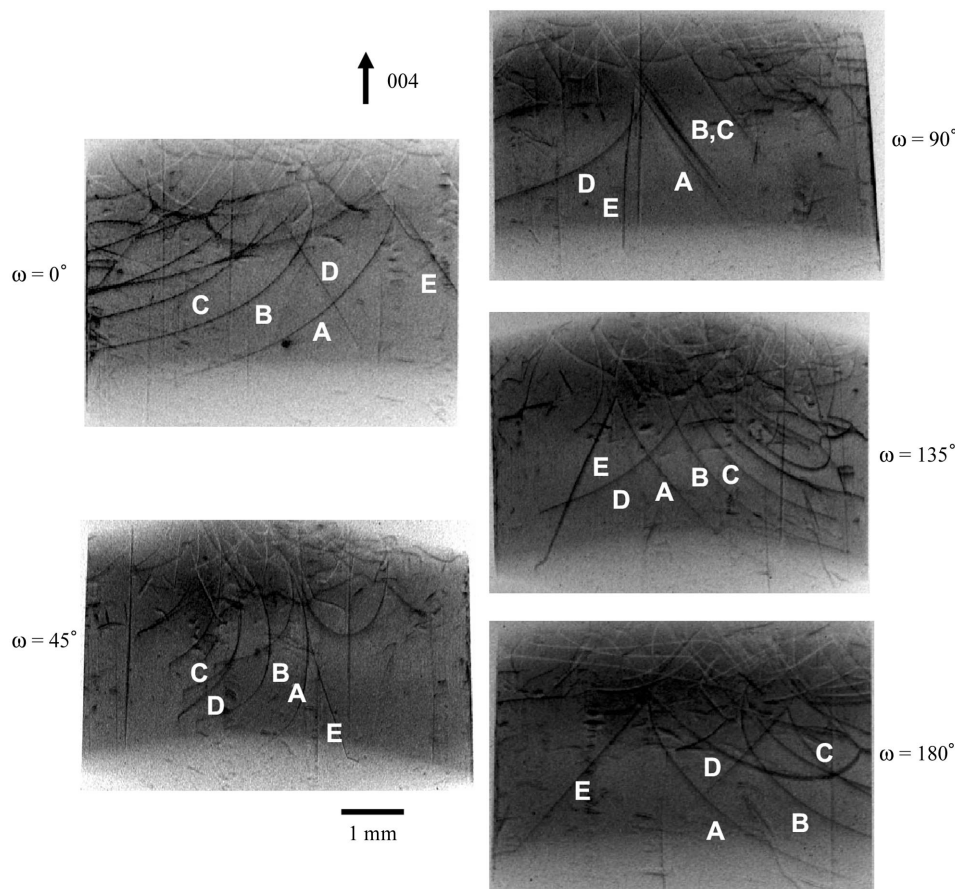

Figure 4
A series of enlarged images in the 004 spot observed at $\omega = 0, 45, 90, 135$ and $180°$. These images were enlarged from X-ray films using an optical microscope.
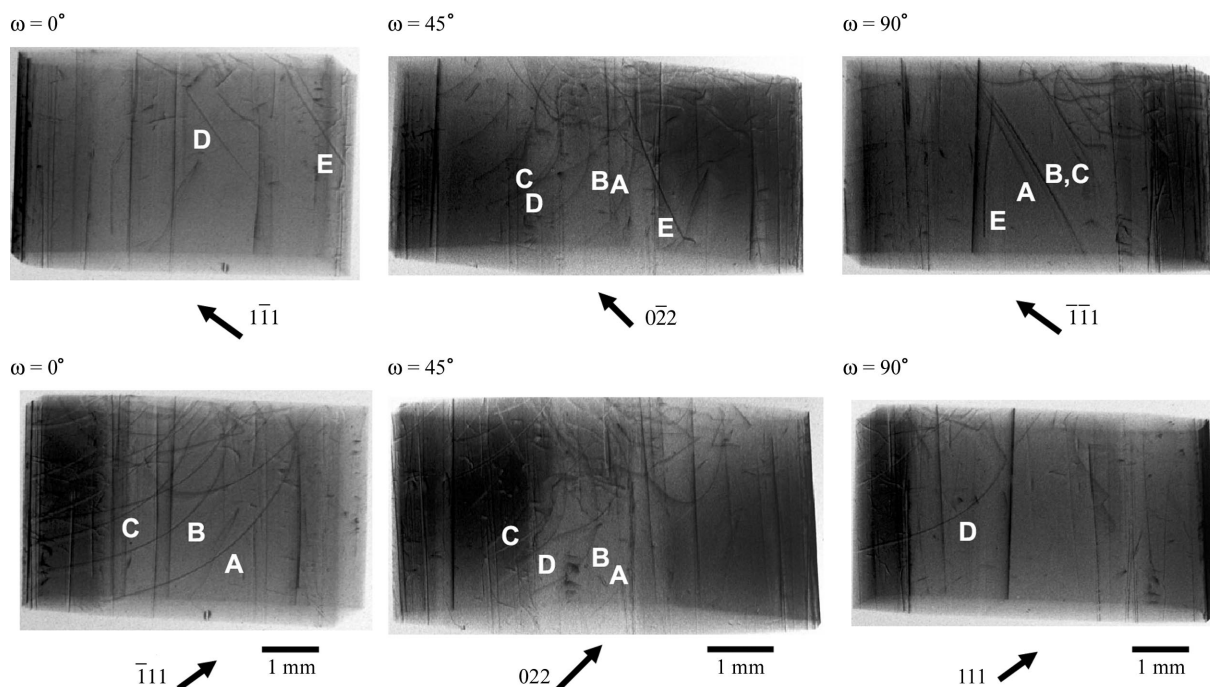
Figure 5
Enlarged images of Laue spots, concerning the {111} and {022} planes, recorded at $\omega = 0$, 45 and 90°, revealing the visibility of dislocations A, B, C, D and E.
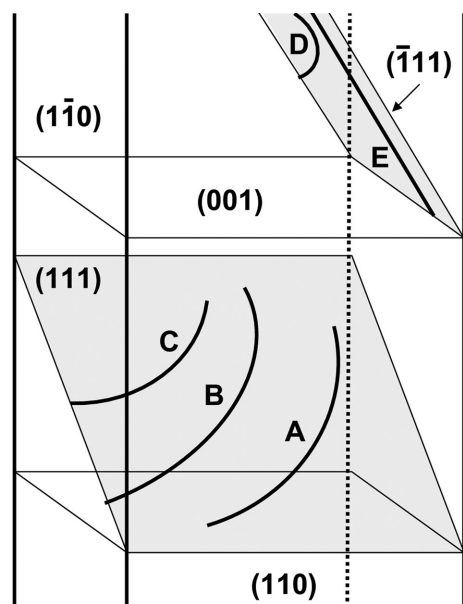

Figure 6
Schematic illustration showing the results of identification of the observed dislocations A to E. Dislocations A, B and C do not lie on the identical (111) plane. Such representation is adopted so as to avoid unnecessary complications. Dislocations D and E are also represented in the same way.

Table 1
Identification of observed dislocations.

Dislocation image	Laue spot		Burgers vector	Glide plane
	Visible	Invisible		
A, B, C	$\bar{1}11$, $\bar{1}\bar{1}1$, $0\bar{2}2$, 022	$1\bar{1}1$, 111	$\mathbf{a}/2[\bar{1}01]$	(111)
D	$1\bar{1}1$, 111, $0\bar{2}2$, 022	$\bar{1}11$, $\bar{1}\bar{1}1$	$\mathbf{a}/2[101]$	$(\bar{1}11)$
E	$1\bar{1}1$, $\bar{1}\bar{1}1$, $0\bar{2}2$	$\bar{1}11$, 022	$\mathbf{a}/2[0\bar{1}1]$	$(\bar{1}11)$

plane of the crystal, *e.g.* {100} and {110}, in order to determine the Burgers vectors of the dislocations. Enlarged topographs are available from the Laue spots concerning the principal lattice planes, *e.g.* {111} and {022}, and consequently the criterion for the image contrast is easily applicable in determining the Burgers vectors. Glide planes can be fixed on the basis of the dislocation configurations and the Burgers vectors.

parallel to the ω-axis, and then to trace the change in the dislocation images in the 004 Laue spot by the ω-rotation, using a CCD camera. Laue topography should be performed at the ω-angle where the incident X-ray beam is almost perpendicular to the principal lattice

References

Andersen, A. L. & Gerward, L. (1974). *Phys. Status Solidi A*, **23**, 537–542.
Authier, A. (2001). *Dynamical Theory of X-ray Diffraction*, ch. 17. Oxford University Press.
Bowen, D. K. & Tanner, B. K. (1998). *High Resolution X-ray Diffractometry and Topography*, ch. 8–10. London: Taylor & Francis.

Chikaura, Y., Iida, S., Kawado, S., Mizuno, K., Kimura, S., Matsui, J., Umeno, M., Ozaki, T., Shimura, T., Suzuki, Y., Izumi, K., Kawasaki, K., Kajiwara, K. & Ishikawa, T. (2001). *J. Phys. D*, **34,** A158–A162.

Haruta, K. (1965). *J. Appl. Phys.* **36**, 1789–1790.

Hirth, J. P. & Lothe, J. (1968). *Theory of Dislocations*, ch. 11. New York: McGraw-Hill.

Imai, Y., Kajiwara, K. & Kato, K. (2003). *BL28B2 White-Beam X-ray Diffraction*, http://www.spring8.or.jp/ENGLISH/facility/bl/PublicBeamline/BL28B2/28b2.html.

Ishikawa, T. (1989). *Rev. Sci. Instrum.* **60**, 2490–2493.

Kawado, S. (2003). *Mater. Sci. Semicond. Process.* **5**, 435–444.

Kawado, S. & Aoyama, J. (1979). *Appl. Phys. Lett.* **34**, 428–429.

Kudo, Y., Liu, K.-Y., Kojima, S., Kawado, S. & Ishikawa, T. (1997). *J. Electrochem. Soc.* **144**, 4035–4041.

Lang, A. R. (1959). *J. Appl. Phys.* **30**, 1748–1755.

Lang, A. R. (1970). *Modern Diffraction and Imaging Techniques in Material Science*, pp. 407–479. Amsterdam: North-Holland.

Lang, A. R. (1999). *International Tables for Crystallography*, Vol. C, pp. 113–123. Dordrecht: Kluwer.

Ludwig, W., Cloetens, P., Härtwig, J., Baruchel, J., Hamelin, B. & Bastie, P. (2001). *J. Appl. Cryst.* **34**, 602–607.

Tanner, B. K. (1976). *X-ray Diffraction Topography*, ch. 4. Oxford: Pergamon.